

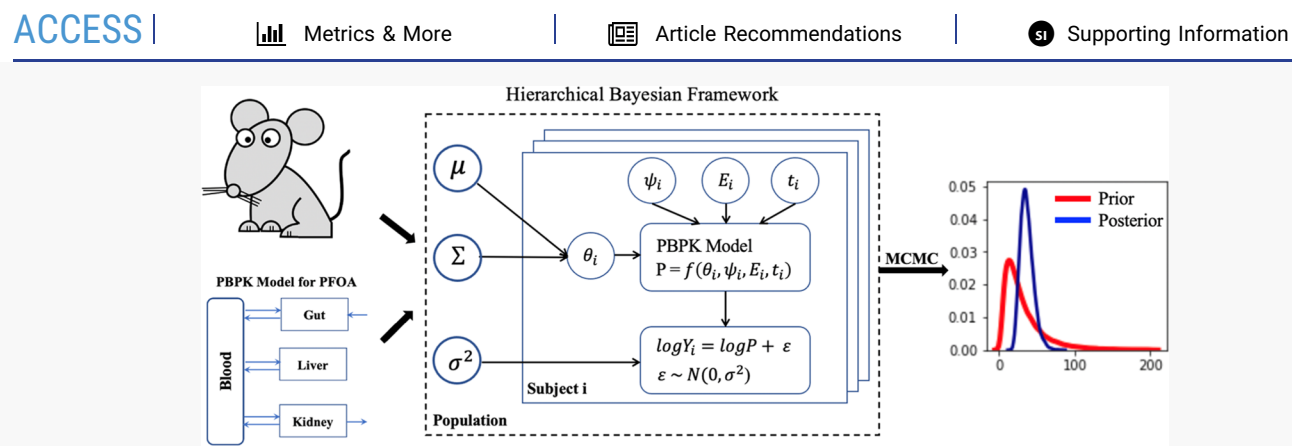
pubs.acs.org/crt Article

# Bayesian Refinement of the Permeability-Limited Physiologically Based Pharmacokinetic Model for Perfluorooctanoic Acid in Male Rats

Weixiao Cheng and Carla A. Ng\*







ABSTRACT: Physiologically based pharmacokinetic (PBPK) modeling is a powerful technique to inform risk assessment of xenobiotic substances such as perfluorooctanoic acid (PFOA). In our previous study, a permeability-limited PBPK model was developed to simulate the toxicokinetics and tissue distribution of PFOA in male rats. However, due to limited information on some key model parameters (e.g., protein binding and active transport rates), the uncertainty of the permeability-limited PBPK model was quite high. To address this issue, a hierarchical Bayesian analysis with Markov chain Monte Carlo (MCMC) was applied to reduce the uncertainty of parameters and improve the performance of the PBPK model. With the optimized posterior parameters, the PBPK model was evaluated by comparing its prediction with experimental data from three different studies. The results show that the uncertainties of the posterior model parameters were reduced substantially. In addition, most of the PBPK model predictions were improved: with the posterior parameters, most of the predicted plasma toxicokinetics (e.g., half-life) and tissue distribution fell well within a factor of 2.0 of the experimental data. Finally, the Bayesian framework could provide insights into the molecular mechanisms driving PFOA toxicokinetics: PFOA-protein binding, membrane permeability, and active transport.

# 1. INTRODUCTION

Perfluorooctanoic acid (C<sub>7</sub>F<sub>15</sub>COOH, PFOA) is one of the most well-studied per- and polyfluoroalkyl substances (PFAS) that were widely used in industrial and consumer products.<sup>1</sup> The wide use of PFOA, however, has caused serious environmental problems and public health concerns.<sup>2</sup> Due to its strong carbon—fluorine bonds, PFOA is highly persistent once in the environment and is hard to be removed, which results in its worldwide presence.<sup>3–5</sup> In addition, experimental studies indicate that PFOA accumulates in the human body, with a biological half-life estimated to be 3.5 years.<sup>6</sup> Epidemiological and animal data show that some toxic effects on the immune system, liver, and endocrine system could be associated with PFOA exposure.<sup>7–9</sup>

The persistence, bioaccumulation, and toxicity of PFOA have received tremendous attention from environmental scientists and regulatory agencies. <sup>10</sup> Especially, a number of physiologically based pharmacokinetic (PBPK) modeling tools

have been developed to inform risk assessment for PFOA in different species such as humans, rats, and monkeys. <sup>11–17</sup> The chemical uptake rate to each tissue assumed by these models is determined by the blood flow rate rather than cell membrane permeability. By neglecting membrane permeability and its associated parameters, the flow-limited assumption simplifies the PBPK model process significantly. However, for chemicals with large molecular weights and/or ionic charges (*e.g.*, PFOA which has a molecular weight of 414.09 Da and is negatively charged at all environmentally and physiologically relevant pH<sup>18</sup>), cell membrane permeability becomes the rate-limiting

Received: May 20, 2021 Published: October 27, 2021





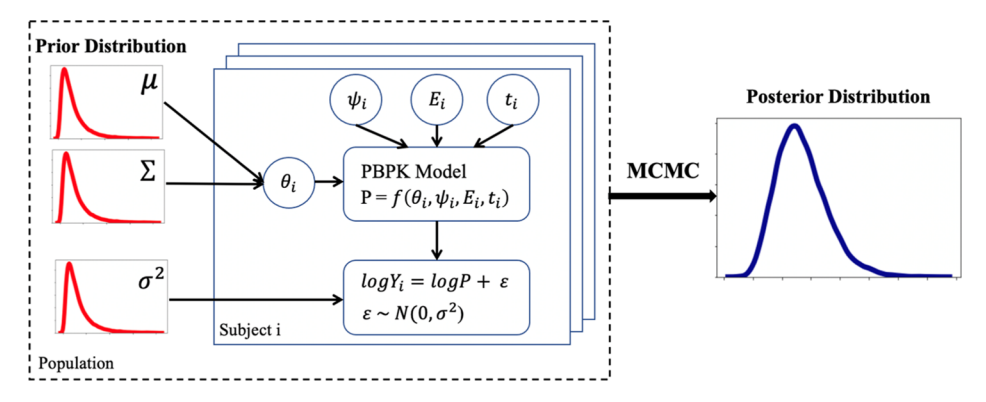


Figure 1. Workflow of hierarchical Bayesian analysis for the permeability limited PBPK model. The PBPK model is a function of chemical-related parameters  $(\theta_i)$ , physiological covariables  $(\psi_i)$ , exposure scenarios  $(E_i)$ , and sampling time points  $(t_i)$ . The individual parameters for each subject i  $(\theta_i)$  are drawn from the population distribution with mean  $(\mu)$  and variance  $(\Sigma)$ . The experimental error term  $(\varepsilon)$  has a normal distribution with mean 0 and variance  $(\sigma^2)$ . Based on the prior information of  $\mu$ ,  $\Sigma$ , and  $\sigma^2$  and experimental data points  $(Y_i)$ , the hierarchical Bayesian framework with MCMC simulations was used to generate the posterior distribution for those parameters.

process for uptake and needs to be included in PBPK models. <sup>19</sup> In addition, none of the current flow-limited models explicitly take the molecular mechanisms for PFOA toxicokinetics (*e.g.*, active transport facilitated by membrane transporters) into consideration, which limits their ability to explain features of the observed PFOA toxicokinetics. Finally, without including membrane permeability, it is hard to build a "bottom up" mechanistic flow-limited model for PFOA. In fact, to the best of our knowledge, all the current flow-limited models require observed *in vivo* data for fitting model parameters (*e.g.*, the resorption maximum and urinary elimination rate) to achieve a satisfactory performance. <sup>11–17</sup> When the *in vivo* data are limited, the flow-limited model may not work well. <sup>15</sup>

Based on the above considerations, we developed a permeability-limited PBPK model that explicitly considers cellular membrane permeability of PFOA through different tissues. 20,21 In addition, our PBPK model included two other important molecular mechanisms for PFOA toxicokinetics: protein binding and active transport processes. Studies have shown that PFOA is strongly bound to serum albumin in plasma and to liver-type fatty acid binding protein (LFABP) in the liver, making them major accumulation sites for PFOA.<sup>22–25</sup> Moreover, active transport facilitated by different transporters is essential to the cellular uptake and efflux of PFOA. 26-29 For example, organic anion transporters and organic anion transporting polypeptides have been reported to play important roles in the renal elimination process of PFOA in humans and rats.<sup>27-29</sup> By incorporating membrane permeability, active transport, and protein binding mechanisms, our PBPK model has been successfully used to estimate the toxicokinetics and tissue distribution of PFOA in both rainbow trout and male rats. 20,21 Moreover, instead of requiring experimental data fitting, all the mechanism-related parameters in the permeability-limited PBPK model were extrapolated from in vitro assays.

However, the major limitation of this PBPK model is that some mechanism-related parameters are either based on a single study (e.g., the equilibrium association constant of PFOA with rat serum albumin) or extrapolated from *in vitro* studies (e.g., active transport rates in the kidney). The limited knowledge about those key parameters leads to a substantial amount of uncertainty in the PBPK model. To address this issue, a hierarchical Bayesian analysis with Markov chain

Monte Carlo (MCMC) was applied to reduce the uncertainty in parameters and improve the performance of the PBPK model.<sup>30</sup>

With prior knowledge on model parameters and measured toxicokinetic data sets, the hierarchical Bayesian framework was used to estimate the posterior distribution of the model parameters. Using the simulated posterior parameters, the PBPK model was then used to estimate the plasma toxicokinetics and tissue distribution of PFOA in male rats. The PBPK model with optimized posterior parameters was evaluated by comparing its prediction with experimental data from three different studies. The Bayesian framework provides a set of more reliable parameters not only for use in PBPK modeling but also to provide insights into the key features of the model structure: PFOA-protein binding, membrane permeability, and active transport.

## 2. MATERIALS AND METHODS

The hierarchical Bayesian approach<sup>34</sup> was employed to reduce the uncertainty and variability of the permeability-limited PBPK model for PFOA in the male rat. The Bayes rule is shown in the following equation<sup>34</sup>

$$P(\theta|Y) = \frac{P(\theta)P(Y|\theta)}{\int P(\theta)P(Y|\theta)d\theta}$$
(1)

where  $\theta$  is the PBPK model parameter vector to be estimated. Y is the measured toxicokinetic data for PFOA.  $P(\theta|Y)$  is the posterior distribution of the model parameters, and  $P(\theta)$  is the prior distribution that describes the prior knowledge of parameters.  $P(Y|\theta)$  is the likelihood of the experimental data set. In order to perform the Bayesian inference, first of all, prior distributions of model parameters need to be defined. Here, we mainly focus on the key parameters that are related to PFOA toxicokinetic mechanisms due to the high uncertainty and sensitivity of those parameters. The prior distributions for those parameters were extrapolated from the literature. Next, the likelihood of the observed data set can be calculated based on the PBPK model. Given the likelihood and prior distribution of the parameter, the posterior distribution for those parameters can be inferred from the Bayes rule. However, it is almost impossible to obtain an analytical expression for  $P(\theta|Y)$ . For this reason, the MCMC technique will be employed to estimate the posterior distribution for the parameters. MCMC is a powerful computational tool to provide samples of parameters without an analytical expression for  $P(\theta|Y)$ .<sup>3</sup>

As indicated in Figure 1, the hierarchical structure consists of two major parts: the subject level and the population level. At the subject

level, for each individual i, the PBPK model (i.e., function f) was used to predict the PFOA concentration—time profiles based on the given parameters including chemical-related parameters ( $\theta_i$ ), physiological covariables ( $\psi_i$ ), exposure scenarios ( $E_i$ ), and sampling time points ( $t_i$ ). The prediction results are related to the experimentally measured concentration data ( $Y_i$ ) through the following error model

$$\log Y_i = \log P + \varepsilon \tag{2}$$

where the error term  $\varepsilon$  is a normal variable with mean set equal to 0 and variance to  $\sigma^2$ . At the population level, to reflect the interindividual variability, chemical-related parameters  $(\theta_i)$  were considered to be generated from a multivariate population distribution, with population mean  $(\mu)$  and variance  $(\Sigma)$ . The prior distribution of the  $\mu$  and  $\Sigma$  for each parameter is discussed in Section 2.2. In this study, we mainly focus on the chemical-related parameters because those parameters are highly sensitive and important to the PBPK model performance; moreover, those parameters have very high uncertainties due to the limited data availability. On the other hand, physiological covariables, such as blood flow rate, tissue volume, and surface area, had more data available and lower model sensitivity according to our previous analysis. These were, thus, fixed in the Bayesian framework to reduce the computational cost in the following simulations.  $^{30,35}$ 

With the prior knowledge of the model parameters and the above hierarchical Bayesian framework, the MCMC technique was employed to numerically estimate the posterior distribution for the model parameters. Finally, the resulting change in the central estimate and the uncertainty and variability of those parameters were analyzed.

In the following sections, the various parts of the workflow including the PBPK model structure, model parameters, experimental data, MCMC simulation, and the analysis of the posterior distributions are described.

**2.1. PBPK Model Structure.** The PBPK model is based on our previous permeability-limited PBPK model for PFOA in male rats, <sup>21</sup> with a single modification to the protein binding process (see Section 2.2.1 for more details) meant to simplify the PBPK model and reduce the computational cost without sacrificing model performance.

Briefly, as shown in Figure S1, based on the physiology of the rat, six tissues including blood, liver, kidney, gut, muscle, and adipose were incorporated in the model. Blood functions as the systemic circulation connecting each compartment together, and it is also a major accumulation site of PFOA. 31-35,36,37 Enterohepatic circulation involving the liver and gut compartments may play an important role in the distribution of PFOA and was thus considered in our model.<sup>38</sup> The kidneys were included because they are primary elimination sites for PFOA.<sup>39</sup> For comparison, muscle and adipose were also added, given the observation that the lowest concentrations of PFOA are found in these tissues.<sup>31,32</sup> Finally, all other compartments were lumped into a single "rest of body" compartment. Each tissue compartment contains both a vascular space and tissue space, the latter of which can be further divided into two subcompartments: an interstitial fluid and a tissue. Three additional compartments including gut lumen, bile, and renal filtrate were also considered to describe the absorption and elimination of PFOA. It is worth mentioning that our PBPK model represents a generic rat because it was compared with the data from both Sprague-Dawley and

After PFOA is orally administered, it is assumed to enter into the gut lumen compartment immediately, where it can be absorbed into the gut tissue. PFOA can then enter into blood, through which it can be transported to other tissues *via* membrane transport. The membrane transport processes include both passive diffusion and active transport facilitated by membrane transporters. For the liver and kidney tissues, active transport involves a number of transporters for uptake and efflux of PFOA (see Section 2.2.2 for details on membrane transport and those transporters). For other tissues, passive diffusion is more important in determining the transport of PFOA because no transporters were reported to be responsible for the transport of PFOA in those tissues. In each tissue, PFOA can bind to different proteins such as serum albumin and LFABP, if they are

present (see Section 2.2.1 for details on protein binding); our model suggests that protein binding processes are mainly responsible for the tissue accumulation of PFOA. Finally, for the elimination of PFOA, the kidney is the major elimination tissue, which involves glomerular filtration, renal clearance, renal reabsorption, and renal efflux processes. Except for glomerular filtration, all these processes are facilitated by membrane transporters (see Section 2.2.2 for more details). PFOA can transport from blood to filtrate *via* glomerular filtration and renal clearance; it can also be reabsorbed from the filtrate back to the tissue compartment through renal reabsorption. Finally, the free fraction of PFOA in kidney tissues could be excreted back into blood *via* the renal efflux process. The other elimination tissue for PFOA is the gut, through fecal excretion.

**2.2. Model Parameters.** The parameters used to support the PBPK model comprise rat physiological parameters and chemical-related parameters. Physiological parameters, including the exchange surface area and the volume for each compartment, blood flow rate, as well as urinary, biliary, and fecal flow rates, are routinely available in the literature for well-studied model species such as the rat, and are summarized in Table S1. For chemical-related parameters, both protein binding and cell membrane transport parameters were considered as the underlying molecular mechanisms controlling PFOA toxicokinetics.<sup>21</sup>

2.2.1. Protein Binding. In terms of the protein binding of PFOA, a total of three proteins were considered: albumin (in blood and interstitial compartments),22 LFABP (in both liver and kidney tissue compartments),  $^{23}_{i}$  and  $\alpha 2\mu$ -globulin (only in the kidney tissue compartment);  $^{40}_{i}$  these proteins have all been demonstrated as important determinants of PFAS accumulation in blood, the liver, and the kidney. In our previous study, 21 the PFOA protein binding was modeled with the binding and dissociation rate constants (i.e., the  $k_{on}$ and  $k_{\text{off}}$ ), the associated mass balance equations are second order differential equations because  $k_{on}$  is a second-order rate constant; the rate of association depends on both the concentration of PFOA and the availability of protein binding sites. To simplify the calculation and reduce the time complexity, in this work we define instead a linear model for the protein binding process.<sup>41</sup> In the linear model (eq 3), the free fraction of PFOA (ff), that is, the ratio of free PFOA concentration ( $C_{\text{free}}$ ) to the total PFOA concentration in tissue  $(C_{total})$ , is determined by the equilibrium association constant (K) and the maximum binding capacity ( $B_{\rm m}$ , which is considered as the total protein concentration in the compartment).

$$ff = \frac{C_{\text{free}}}{C_{\text{total}}} = \frac{1}{1 + K \times B_{\text{m}}}$$
(3)

Here, if is considered to be independent of  $C_{\rm free}$  and the protein binding of PFOA is therefore characterized by a constant parameter predefined by K and  $B_{\rm m}$ . The K of albumin, LFABP, and  $\alpha 2\mu$ -globulin as well as the concentration of those proteins in different tissues (i.e.,  $B_{\rm m}$ ) were obtained from the literature and are shown in Tables S2 and S3. With the free fraction parameter, the corresponding mass balance equations become first-order differential equations (Supporting Information Section S3). The linear binding model is able to generate similar simulation results to the previous model, but its running time is significantly improved, making the MCMC simulation more cost-effective.

2.2.2. Membrane Transport. Both passive diffusion and active transport facilitated by proteins play essential roles in membrane transport of PFOA.  $^{20,21,27,38,42}$  To derive the mass balance equations for those processes, passive diffusion rates for each tissue and active transport rates for each relevant membrane transporter are required. For passive diffusion, the effective permeability ( $P_{\rm eff}$ ) for each tissue was used to calculate the passive diffusion rate. As shown in eq 4, permeability is estimated based on Fick's law

$$P_{\text{eff}} = \frac{J}{A\Delta C} \tag{4}$$

where J, the initial passive diffusion flux, was empirically determined by extracting *in vitro* data from Weaver *et al*;<sup>27</sup> the average value of J

is around 0.13 nmol/mg protein/min and is converted to mol/s by scaling to the protein content of each tissue-specific cell type (Table S2). A is the cellular surface area, which is assumed to be 4000  $\mu$ m<sup>2</sup> for a single cell.<sup>20</sup>  $\Delta C$  is the concentration of PFOA in the exposure medium (*i.e.*, 10  $\mu$ mol/L in the Weaver *et al.* study).<sup>27</sup>

Once  $P_{\rm eff}$  is determined, the passive diffusion rate (k) between the connected tissue compartments can be calculated as follows.

For diffusion between blood (B) and the interstitial fluid compartment in each tissue (iF)

$$k^{\text{iF-B}} = k^{\text{B-iF}} = \left(\frac{1}{Q_{\text{B}}^{i}} + \frac{1}{P_{\text{eff}}^{\text{B}} A^{\text{B-iF}}}\right)^{-1}$$
 (5)

where  $Q_{\rm B}^{\rm i}$  is the blood flow to each tissue, and  $A^{\rm B-iF}$  is the surface area of exchange between blood and the fluid compartment (Table S1).

For diffusion between the fluid (iF) and tissue (iT) subcompartment in each tissue, only permeability accounts for the overall mass transfer

$$k^{iF-iT} = k^{iT-iF} = P_{eff}^{i} A^{iF-iT}$$
(6)

For tissues containing the filtrate, bile, or gut lumen, the diffusion between tissues and those subcompartments (iS) is calculated by

$$k^{iS-iT} = P_{\text{eff}}^{i} A^{iS-iT} \tag{7}$$

$$k^{\text{iT-iS}} = \frac{k^{\text{iS-iT}}}{\text{CR}_{\text{ss}}^{\text{C-W}}} \tag{8}$$

where  $CR_{ss}^{C-W}$  is the steady-state cell—water concentration ratio, which can be extrapolated from *in vitro* data.<sup>20</sup> The values of  $CR_{ss}^{C-W}$  for liver to bile, kidney to filtrate, and enterocyte to gut lumen are shown in Table S4.

Regarding active transport, a total of five transporters including organic anion transporters (Oat1 and Oat3),<sup>27</sup> an organic anion transporting polypeptide (Oatp1a1),<sup>27</sup> the organic solute and steroid transporter  $(\operatorname{Ost}\alpha/\beta)$ , 38 and Na<sup>+</sup>/taurocholate cotransporting polypeptide (Ntcp)<sup>38</sup> were used to characterize the active cellular uptake and efflux of PFOA. These transporters are responsible for four active transport processes: (i) renal clearance, which involves Oat1 and Oat3 located at the basolateral membrane of proximal tubular cells; (ii) renal reabsorption, which involves Oatp1a1 located at the apical membrane of proximal tubular cells; (iii) renal efflux, which relates to Ost $\alpha/\beta$  located at the basolateral membrane of proximal tubular cells; and (iv) hepatocyte uptake, which relates to Oatp1a1 and Ntcp located at the basolateral membrane of hepatocytes.<sup>39</sup> Similar to the passive diffusion process, Fick's law was used to derive the coefficients for those four active transport processes; the only difference is that the I parameter in eq 4 corresponds to the flux of transporter-expressing cell rather than the passive diffusion flux. The J value for each transporter and the calculated active transport coefficients are shown in Table S5. Finally, the active transport rate for each process can be derived by multiplying the transport coefficient by the surface area for exchange of the corresponding tissue.

2.2.3. Prior Distributions. As described above, many parameters are involved in the PBPK model (68 in all). To reduce the computational cost for the MCMC simulation, only the chemical-related parameters to which the model was previously shown to be most sensitive<sup>21</sup> were selected for the uncertainty analysis. In our previous study, Monte Carlo methods were used to conduct the sensitivity analysis. Briefly, all the model parameters were sampled from their prior distributions (10 000 samples were taken for each parameter) and then used to run the PBPK model. Finally, correlation analysis was performed between sampled parameters and model predictions of PFOA concentrations. A high correlation coefficient indicates a parameter to which the model is highly sensitive. Based on the correlation analysis results, these highly sensitive parameters include protein binding parameters: the equilibrium association constants, K, between PFOA and albumin and LFABP; passive diffusion parameters:  $P_{\rm eff}$  of blood, the liver and kidney, CR $_{\rm ss}^{\rm C-W}$  of the liver and kidney; and active transport parameters: active transport rates of the four active transport

processes discussed above (Table 1). Other parameters, such as physiological parameters, K of  $\alpha 2\mu$ -globulin, and  $P_{\rm eff}$  of gut, muscle

Table 1. Summary of the Parameters of the PBPK Model Selected for MCMC Analysis  $^a$ 

parameters	symbol	values	unit	confidence factor (Cf)
effective permeability of blood	$P_{ m eff}^{ m B}$	0.18	mm/h	5
effective permeability of kidney	$P_{ m eff}^{ m K}$	0.16	mm/h	5
effective permeability of liver	$P_{ m eff}^{ m L}$	0.19	mm/h	5
steady-state cell—water concentration ratio of kidney	$CR_{ss}^{K}$	6.2	unitless	5
steady-state cell—water concentration ratio of liver	$CR_{ss}^{L}$	7.3	unitless	5
renal clearance rate constant	$P_{ m b}^{ m clear}$	0.99	mm/h	5
renal reabsorption rate constant	$P_{ m b}^{ m reab}$	0.43	mm/h	5
renal efflux rate constant	$P_{ m b}^{ m efflux}$	0.50	mm/h	5
hepatocyte uptake rate constant	$P_{ m b}^{ m uptake}$	0.64	mm/h	5
association constant of albumin	$K_{\rm a}$	$2.4 \times 10^4$	$M^{-1}$	5
association constant of LFABP	$K_{ m LFABP}$	$1.4 \times 10^{5}$	$M^{-1}$	5

"For the association constants, the values represent measured association constants multiplied by the number of binding sites.

and adipose, were considered as fixed values in the hierarchical Bayesian framework because those parameters were well-studied (low uncertainty) or had much less influence on the model performance.<sup>21</sup>

Next, as described in Figure 1, the population mean  $(\mu)$  of each selected parameter was assigned with a log-normal prior distribution with hyperparameter mean (M) and standard deviation (S). The M value for each parameter was derived from the literature, as shown in Table 1; the S value was calculated based on equation:  $S = e^{1/2\ln(Cf)}$ , where Cf represents confidence factor, which is an intuitive measure of variance in log-normal distributions. For example, a Cf of 2 indicates that 95% of the values lie between 1/2 and 2 times the median. Given the scarcity of the available data for those parameters, a value of S was assigned for them, indicating the high uncertainty of their prior distributions (Table 1).

The prior distributions assigned to the population variance of those parameters ( $\Sigma^2$ ) were inverse gamma distribution:  $\Sigma^2 \sim \text{InvGamma-}(\alpha, \beta)$ , where the shape parameter  $\alpha$  is set to 3, and the scale parameter  $\beta$  is set to 0.5 based on previous studies. The quantities M, S,  $\alpha$  and  $\beta$  are hyperparameters that embody prior knowledge of the uncertainty and variability of the model parameters.

Finally, considering the high uncertainty and variation of experimental data among different studies (e.g., 1 mg PFOA/kg BW IV and oral dose scenarios from the Kemper  $^{31}$  and the Kim et al.  $^{33}$  studies), the prior distribution of the experimental error term ( $\sigma^2$ ) was modeled as a noninformative uniform distribution with a lower bound of 0.01 and upper bound of 3.3 for all experimental measurements.  $^{30,35}$ 

**2.3. Experimental Data.** Several experimental studies have reported toxicokinetics and tissue distribution of PFOA in male rats. As summarized in Table 2, a total of seven data sets from three studies were collected that cover different administration routes, dose scenarios, sampling time of each tissue and rat species. All concentration data were taken directly from tables or extracted from plots with the WebPlotDigitizer tool (https://automeris.io/WebPlotDigitizer/).

Table 2. Summary of PFOA Toxicokinetics Studies for Male Rats

administration routes	dose scenarios	sampling time for tissues	rat species	references
single oral	1 mg/kg	sample from blood at 0.25, 0.5, 1, 2, 4, 8, 12, 16, 24, 36, 48, 72, 96, 120, 144, 168, 192, 240, 288, 336, 384, 432, 480, 528 h	Sprague-Dawley	Kemper <sup>31</sup>
single oral	0.1 mg/kg			
single IV	1 mg/kg			
single oral	1 mg/kg	sample from liver, kidney, gut, muscle and adipose after 672 h		
single oral	1 mg/kg	sample from blood at 6, 12, 24, 48, 96, 144, 192, 240, 288 h; sample from liver and kidney after $288\ h$	Sprague-Dawley	Kim et al. <sup>33</sup>
single IV	1 mg/kg			
single IV	0.041 mg/kg	sample from blood at 5, 15, 45, 90, 120, 150, 210, 270, 300 min; sample from liver, kidney, gut and adipose after 120 min	Wistar	Kudo et al. <sup>32</sup>

Table 3. Percentiles of the Prior and Posterior Distribution for Each Parameter

	prior distribution			posterior distribution		
parameters	2.50%	50%	97.50%	2.50%	50%	97.50%
$P_{ m eff}^{ m B}$	0.037	0.18	0.87	0.56	0.79	0.87
$P_{ m eff}^{ m K}$	0.033	0.16	0.76	0.038	0.19	0.67
$P_{ m eff}^{ m L}$	0.038	0.19	0.9	0.042	0.19	0.83
$CR_{ss}^{L}$	1.5	7.3	35	1.6	7.7	33
$CR_{ss}^{K}$	1.3	6.2	30	1.5	6.8	26
$P_{ m b}^{ m clear}$	0.21	0.99	4.8	0.3	1.7	4.6
$P_{ m b}^{ m reab}$	0.088	0.43	2.1	0.094	0.23	1.4
$P_{ m b}^{ m uptake}$	0.13	0.64	3.1	0.14	0.34	2.3
$P_{ m b}^{ m efflux}$	0.1	0.5	2.4	0.11	0.27	1.2
$K_{\rm a}$	$5.0 \times 10^{3}$	$2.4 \times 10^{4}$	$1.2 \times 10^{5}$	$2.3 \times 10^{4}$	$3.6 \times 10^{4}$	$5.7 \times 10^4$
$K_{ m LFABP}$	$2.8 \times 10^{4}$	$1.4 \times 10^{5}$	$6.5 \times 10^5$	$3.3 \times 10^4$	$1.4 \times 10^{5}$	$4.8 \times 10^{5}$

2.4. MCMC Simulation. With the prior information of the population mean  $(\mu)$  and variance  $(\Sigma^2)$  and experimental error term  $(\sigma^2)$ , the joint posterior distribution given the experimental data (Y)can be determined based on Bayes' theorem, as shown in eq 9.3

$$p(\theta, \mu, \Sigma^2, \sigma^2 | Y) \propto p(Y | \theta, \sigma^2) \times p(\theta | \mu, \Sigma^2) \times p(\mu) \times p(\Sigma^2)$$
  
  $\times p(\sigma^2)$  (9)

 $p(\mu)$ ,  $p(\Sigma^2)$ , and  $p(\sigma^2)$  are the probabilities calculated from corresponding prior distributions.  $p(\theta|\mu, \Sigma^2)$  is the probability of an individual chemical-related parameter  $\theta$ , which is assumed to be lognormally distributed as  $\log(\theta) \sim N(\log(\mu), \Sigma^2)$ . Finally,  $p(Y|\theta, \sigma^2)$  is the likelihood of the experimental data Y, which is determined based on  $\log(Y) \sim N(\log(P), \sigma^2)$ , where P is the predicted concentration time data from the PBPK model given a set of parameters (i.e., P =  $f(\theta, \psi, E, t)$ , as in Figure 1).

Due to the nonlinearity of the PBPK model, it is impossible to acquire an analytical expression for  $p(\theta, \mu, \Sigma^2, \sigma^2|Y)$ . Instead, the Delayed Rejection Adaptive Metropolis (DRAM) algorithm, 44 a commonly used MCMC sampling technique, was employed to numerically approximate the joint posterior distribution. DRAM was selected because it is highly efficient and has been successfully applied in toxicokinetic models.<sup>30</sup> Here, a total of four Markov chains were constructed in the simulation. For each chain, the total number of iterations was set to 300 000, with the first 150 000 iterations as a "burn-in" period and the last 50 000 iterations as the output samples for posterior distribution analysis.

2.5. Posterior Analysis and Evaluation. After an MCMC simulation, the convergence of the posterior distributions needs to be verified before further analysis. The Gelman-Rubin diagnostic was used to assess the samples generated from the MCMC method.<sup>45</sup> Specifically, the potential scale reduction factor (PSRF)  $(\hat{R})$  was calculated for each parameter distribution. When the posterior distribution becomes stationary,  $\hat{R}$  is close to 1. An  $\hat{R}$  value of 1.2 or less is considered to be converged for the distribution, as recommended by Gelman et al.

Based on the MCMC output, the posterior quantiles and density plots for the distribution of each selected model parameter were generated for analysis. The PBPK model was then rerun with the updated parameter distributions and its output was compared with prior model results. Finally, based on the new predicted concentration-time data, toxicokinetic parameters including halflife, clearance, the maximum PFOA concentration in plasma  $(C_{max})$ , and the time required to reach the peak concentration  $(T_{max})$  were calculated and compared with experimental data from other studies. For the calculation of half-life  $(T_{1/2})$ , we employed the first order elimination rate (K<sub>e</sub>), which is determined by considering the elimination phase after  $C_{\rm max}$  and  $T_{\rm max}$ . Specifically, the following equations were used to calculate the half-life value<sup>47</sup>

$$T_{1/2} = \frac{\ln(2)}{K_{\rm e}} \tag{10}$$

$$K_{\rm e} = -\frac{\ln(C_{\rm end}) - \ln(C_{\rm max})}{T_{\rm end} - T_{\rm max}}$$
 (11)

where  $C_{\rm end}$  and  $T_{\rm end}$  represent the concentration of PFOA and the time at the end point, respectively. The following equation was used to calculate clearance<sup>4</sup>

$$clearance = \frac{dose}{AUC}$$
 (12)

where AUC is the area under the curve.

2.6. Software and Model Code. The PBPK model and MCMC simulation were programmed in R (https://www.r-project.org/) using mrgsolve (https://mrgsolve.github.io/), a package designed for solving ordinary differential equations, for the PBPK model development. The MCMC simulation was coded using the FME package, which provides convenient functions for the DRAM algorithm. 48 All model codes are available in the Supporting Information.

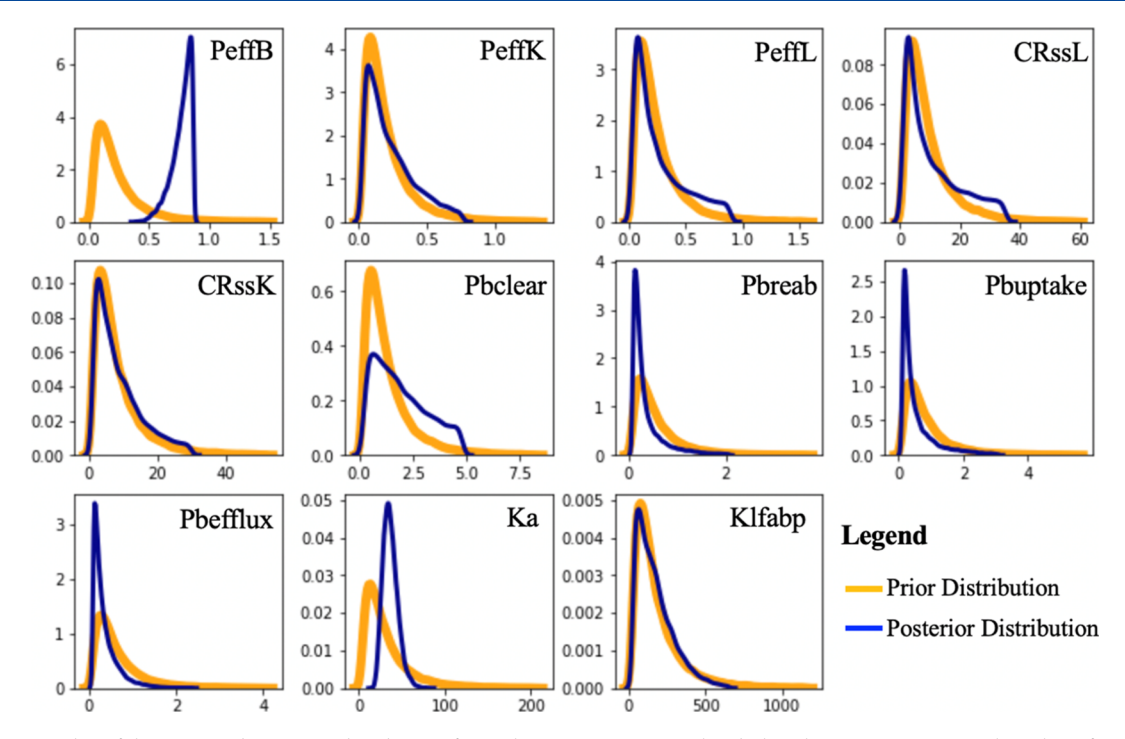


Figure 2. Density plot of the prior and posterior distribution for each parameter. For each subplot, the *x*-axis represents the value of each parameter (the unit for  $K_a$  and  $K_{LFABP}$  is  $m^3/mol$ ,  $CR_{ss}^L$  and  $CR_{ss}^K$  are unitless, and the remaining parameters have units of mm/h); the *y*-axis represents the probability density.

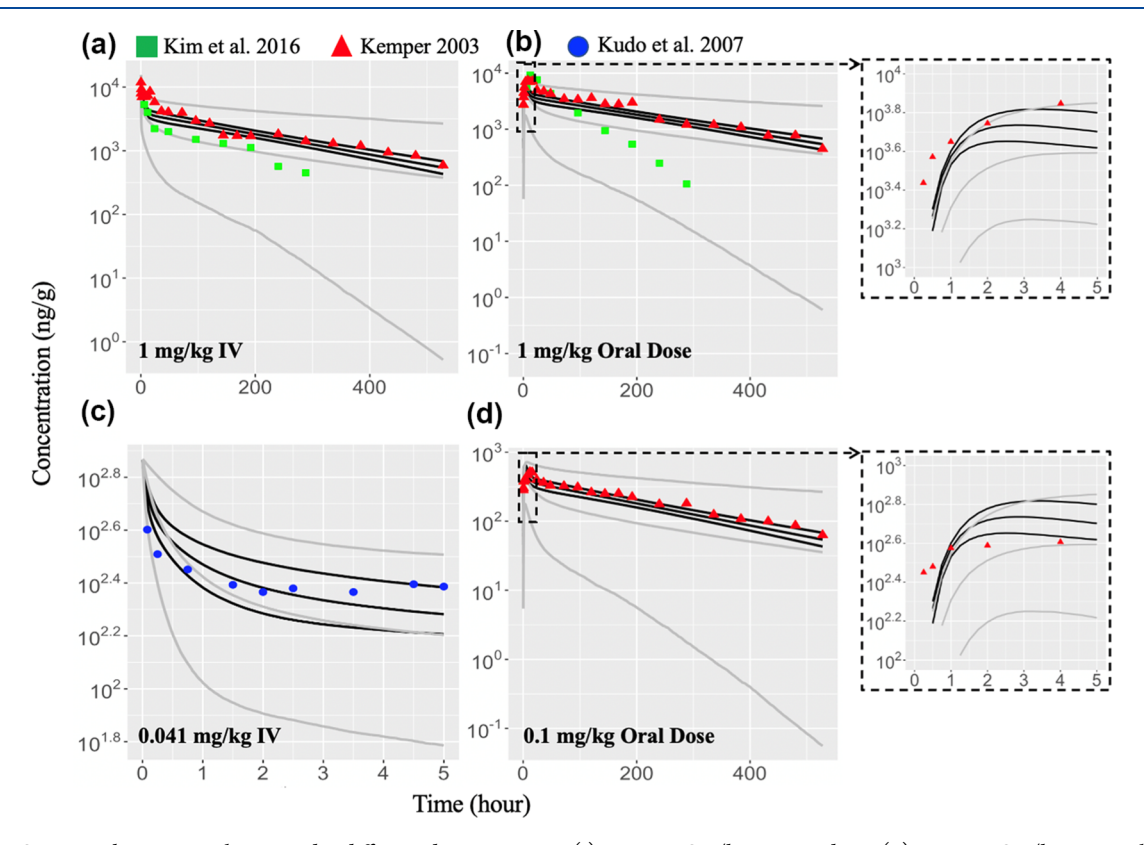


Figure 3. PFOA toxicokinetics in plasma under different dose scenarios: (i) 1 mg PFOA/kg BW IV dose; (ii) 1 mg PFOA/kg BW oral dose; (iii) 0.041 mg PFOA/kg BW IV dose; (iv) 0.1 mg PFOA/kg BW oral dose. The gray line represents model results using prior parameter distributions; the black line is with the posterior distributions. The upper, middle, and lower lines indicate the 97.5th, 50th, and 2.5th percentiles of the predicted results, respectively. Red triangles, green squares, and blue circles represent the data sets extracted from the works of Kemper 2003, Kim et al. 2016, and Kudo et al. 2007, respectively. The first 5 h time-course behavior for oral dose was zoomed in to show its upward trend at the beginning phase.

Table 4. Comparison of Toxicokinetic Parameters between Model Predictions and the Kemper Data<sup>31</sup>

dose scenario		half-life (day) clearance (mL/day/kg)		$C_{\text{max}} (ng/g)$	$T_{\rm max}$ (h)	
0.1 mg/kg oral	prior	14.74 ± 15.55	69.31 ± 71.96	424 ± 147	5.15 ± 3.32	
	posterior	$7.9 \pm 0.66$	$26.95 \pm 1.72$	$546 \pm 50.9$	$2.87 \pm 0.26$	
	Kemper data	$8.41 \pm 1.56$	$23.10 \pm 5.76$	$598 \pm 127$	$10.25 \pm 6.45$	
1 mg/kg oral	prior	$15.22 \pm 19.86$	$65.83 \pm 71.66$	$4246 \pm 146$	$5.1 \pm 3.11$	
	posterior	$7.91 \pm 0.67$	$25.18 \pm 1.55$	$5479 \pm 532$	$2.89 \pm 0.27$	
	Kemper data	$5.76 \pm 1.33$	$20.9 \pm 3.79$	8431 ± 1161	$9.0 \pm 3.83$	
1 mg/kg IV	prior	$15.41 \pm 17.52$	$68.78 \pm 91.51$			
	posterior	$7.89 \pm 0.67$	$24.99 \pm 1.55$			
	Kemper data	$7.73 \pm 0.82$	$21.51 \pm 1.97$			

## 3. RESULTS

**3.1. Convergence Diagnosis.** The trace plots for Markov chains in MCMC are shown in Figures S2–S4. As indicated, no visible trends or changes were observed in the trace plot for each model parameter, suggesting good convergence of the distribution for each parameter. In addition, the Gelman–Rubin diagnostic results (Table S6) show that all parameters have PSRF values between 1.001 and 1.02, with upper confidence limits between 1.002 and 1.056. The multivariate PSRF value, which forms the upper bound of PSRF for any linear combination of the parameters, is 1.09. All PSRF values are less than 1.2, indicating the posterior distributions in MCMC have reached equilibrium and can be used for further analysis.

3.2. Parameter Analysis. The percentile (2.5, 50 and 97.5%) and density plot comparisons between prior and posterior distribution for each model parameter are shown in Table 3 and Figure 2, respectively. After updating with experimental data, the posterior distributions of the population mean for all parameters were substantially narrower than their prior distributions, indicating that the uncertainties of those parameters were substantially reduced. In addition, an obvious shift was observed in the density plot for some parameters (e.g.,  $P_{\text{eff}}^{\text{B}}$  and  $K_{\text{a}}$  in Figure 2). The percentiles of distributions also showed significant changes (defined by larger than ±20% of prior values<sup>49</sup>) between prior and posterior values for some parameters. Specifically, the posterior median of the effective permeability of blood vessels ( $P_{\text{eff}}^{\text{B}}$ ) is 0.79 mm/h, which is 4.4 times higher than its prior median. In addition, the posterior median of the  $K_2$  value (i.e., the association constant of albumin multiplied by the number of binding sites) is  $3.6 \times 10^4 \text{ M}^{-1}$ , which is increased by 48% compared to its prior median. Finally, the posterior medians of all the active transport parameters were substantially different from their prior values: after updating with experimental data, the renal clearance rate constant ( $P_b^{clear}$ , 1.7 mm/h) increased by 71.5%; the hepatocyte uptake rate constant ( $P_{\rm b}^{\rm uptake}$ , 0.34 mm/h), renal reabsorption rate  $(P_b^{\text{reab}}, 0.23 \text{ mm/h})$ , and renal efflux rate constant  $(P_b^{\text{efflux}},$ 0.27 mm/h) decreased by 47.4, 46.4, and 46.3%, respectively. Finally, the effective permeability of the kidney and liver (i.e.,  $P_{\text{eff}}^{\text{K}}$  and  $P_{\text{eff}}^{\text{L}}$ ), steady-state cell—water concentration ratio of the kidney and liver (i.e., CR<sub>ss</sub> and CR<sub>ss</sub>), and the association constant of LFABP (i.e., K<sub>LFABP</sub>) indicate posterior median of 0.19 mm/h, 0.19 mm/h, 7.7, 6.8, and 1.4  $\times$  10<sup>5</sup> M<sup>-1</sup>, respectively. No significant changes were observed for these medians between their prior and posterior distributions, which indicates that the prior information of these parameters agree very well with the experimental toxicokinetics data.

**3.3. Model Evaluation.** The PBPK model was rerun with the generated posterior parameter distribution and its results

were evaluated by comparing with both experimental toxicokinetic data and model predictions based on prior parameter information. The model evaluation for plasma toxicokinetics and tissue distribution are described below.

3.3.1. Plasma Toxicokinetics. As shown in Figure 3, both prior and posterior model predictions indicated a similar timecourse behavior to the experimental data. However, the 95% range of the posterior prediction (black line) was substantially smaller than that of the prior prediction (gray line), demonstrating a significant decrease in the model uncertainty. In addition, most experimental data fall within the 95% range of the posterior prediction of PFOA concentration in plasma, except for data from the Kim et al. study,<sup>33</sup> which show a higher elimination rate. It is worth noting that even under the same dose scenarios (e.g., 1 mg PFOA/kg BW IV and oral dose), the PFOA concentration profiles are quite different between Kim et al.<sup>33</sup> and the Kemper study.<sup>31</sup> One reason for the substantial difference could be due to the different analytical methods used to measure PFOA concentration. In the Kemper study, standard liquid chromatography-mass spectrometry was used to detect the PFOA concentration in plasma. By the time of the Kim et al. study, 2 newer ultrahighperformance liquid chromatography-coupled tandem mass spectrometry had become the standard, a more sensitive method for PFAS analysis. In addition, the Kim et al. study dosed three different PFAS simultaneously-PFOA, PFOS, and PFHxS, and it is therefore possible that the presence of the other PFAS affected the toxicokinetics of PFOA. The differences in PFOA concentration profiles observed under the same dose for PFOA illustrate the significant variation that can be found across experimental toxicokinetic studies. In the case of these two studies, this is potentially problematic because an older study with a larger number of data points biases the model away from fitting a newer study with fewer data points that may use a more reliable analytical method. Given the differences in dosing (single vs multiple PFAS), however, it is difficult to say definitively which is more reliable.

Finally, based on the predicted PFOA concentration profiles in plasma, different toxicokinetic parameters were estimated and compared with the experimental results from the Kemper study (*i.e.*, the Kemper data). As shown in Table 4, in comparison with the Kemper data, the posterior model results demonstrate much improvement from the prior model for the half-life, clearance of PFOA, and maximum plasma concentration of PFOA ( $C_{\rm max}$ ); the posterior predicted values for those toxicokinetic parameters fall well within a factor of 1.5 of the Kemper data for three different dose scenarios. The half-life seems to be independent of dose scenarios and is calculated as 7.90 days, which is in very good agreement with the half-life values from other experimental studies (range from 5.63 to 15

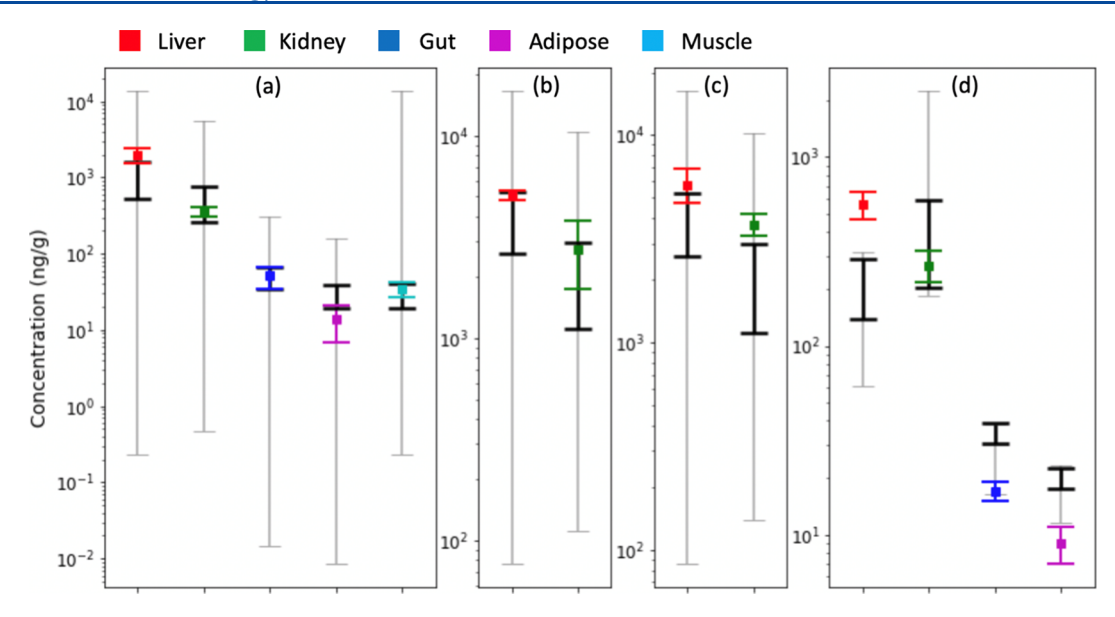


Figure 4. PFOA terminal tissue distribution under different dose scenarios. (a) 28 days after 1 mg PFOA/kg BW oral dose; (b) 12 days after 1 mg PFOA/kg BW IV dose; (c) 12 days after 1 mg PFOA/kg BW oral dose; (d) 2 h after 0.041 mg PFOA/kg BW IV dose. The grey and black lines represent the 95% range of the model predictions using prior and posterior parameter distributions, respectively. Color bars are experimental data sets from different studies (a: Kemper 2003, b and c: Kim et al. 2016, and d: Kudo et al. 2007) All experimental data are shown as mean ± standard deviation.

days).  $^{50-53}$  The posterior clearance of PFOA is also very similar under different dose cases and has an average value of 25.70 mL/day/kg, which falls within the range of other experimental data (from 21.5 to 50.5 mL/day/kg).  $^{50,52,54}$  For the time required to reach the maximum concentration ( $T_{\rm max}$ ), the prior and posterior model predictions are underestimated by a factor of around 2 and 3.5, respectively. The major reason for the underestimation of  $T_{\rm max}$  is due to a simplification of the absorption process for PFOA. In our PBPK model, it is assumed that orally administrated PFOA enters into the gut lumen immediately; however, in reality, it could take some time for PFOA to reach the small intestine. This simplifying assumption was made due to the limited data available on the absorption of PFOA.

3.3.2. Tissue Distribution. Figures 4 and S5–S7 show the comparison of PFOA tissue distribution between model predictions (with both prior and posterior parameter distributions) and experimental results under different dose scenarios. As indicated in Figure 4, our model was able to successfully predict the tissue distribution patterns for PFOA in long-term simulations (i.e., after 12 or 28 days): liver > kidney > gut > muscle  $\approx$  adipose. For a short-term dosing scenario (e.g., 2 h), the predicted PFOA concentration in liver was significantly lower than the measured data. Similar to the plasma toxicokinetics results, the uncertainty for posterior model predictions was reduced substantially compared with the prior model. Most measured PFOA concentrations in each tissue fall well within or overlap with the 95% prediction range, except for the data from the Kudo et al. study.  $^{32}$ 

A further comparison was performed between the means of experimental data in different tissues and the means of the model predictions. For long-term simulations, the posterior model predictions are well within a factor of two of measured concentrations for both oral and IV dose. For short-term dosing (*i.e.*, the Kudo *et al.* study<sup>32</sup>), the hepatic PFOA concentration was underestimated by the PBPK model but is within a factor of 2.6.

## 4. DISCUSSION

In this study, we further strengthened our permeability-limited PBPK model for PFOA in the male rat with the hierarchical Bayesian framework. By incorporating measured PFOA toxicokinetics data, the MCMC technique was able to generate improved posterior distributions for key model parameters. With the help of this statistical framework, not only were the uncertainties of the posterior parameters substantially reduced but most of the PBPK model predictions also became more reliable and meaningful (e.g., the toxicokinetic parameters such as half-life and clearance of PFOA estimated with posterior parameters are well within a factor of 1.5 of the experimental data, while the prior calculated toxicokinetic parameters fall within a factor of 1.8 to 3.2 of the experimental data), thus improving the risk assessment of PFOA. Although the PBPK model using the posterior parameters demonstrates better performance than the prior model, it is worth pointing out that this is because the Bayesian framework used the experimental data to update the parameter distributions. In other words, the applicability of the posterior model relies on the accuracy of the available experimental data sets. If one of these data sets turn out to be unreliable, it may be tuning the model in the wrong direction. As indicated in Figure 3, there are substantial differences between the experimental data from the Kim et al.33 and Kemper studies.<sup>31</sup> In addition, the Kemper study has more data points (72 data points) than the Kim et al. study (18 data points). Because the Bayesian framework is a data-driven technique and its performance is closely associated with the data sets, the posterior model fit better with the Kemper study (which has many more data points), while most of the Kim et al. data fall outside the 95% range of the model prediction. On the other hand, the prior PBPK model, while it has high uncertainty, relies on no in vivo toxicokinetics data and thus could be less subject to bias. However, by building this MCMC framework, we make it possible to continuously upgrade the performance of the toxicokinetic model as more high-quality data become available, and this can apply to both in vitro parameter data and *in vivo* toxicokinetic data. For example, if more toxicokinetic data become available, the MCMC analysis will lead to less biased results and therefore less biased posterior distributions for key parameters. On the other hand, if more parameter data become available, the posterior distributions can be compared with the newly established values to determine whether toxicokinetic data are biasing the distributions in the wrong direction and thereby drive decisions to eliminate those datasets from the analysis.

**4.1. Toxicokinetics of PFOA.** The Bayesian statistical framework provided more insights into the molecular mechanisms that result in the observed PFOA toxicokinetics. As indicated in Table 3, the posterior median of the association constant for albumin  $(K_a)$  increased substantially compared to its prior value. It is worth pointing out that only one study was available for the prior knowledge of  $K_a$  in rats, and its association constant value  $(3.1 \times 10^3 \text{ M}^{-1} \times 7.8 \text{ binding sites}^{22})$  is much smaller compared with the  $K_a$  values in humans  $(e.g., 3.12 \times 10^4 \text{ M}^{-1} \times 13 \text{ binding sites}^{55} \text{ and } 1.26 \times 10^4 \text{ M}^{-1} \times 2.4 \text{ binding sites}^{24})$  and bovines  $(e.g., 4.36 \times 10^4 \text{ M}^{-1} \times 1 \text{ binding sites}^{56})$ . Both our model predictions and the comparison with other experimental data seem to indicate the current  $K_a$  value for rat is a little low and more studies are needed to measure  $K_a$  for PFOA with rat serum albumin.

Another important insight is about the renal elimination of PFOA. From Table 4, compared with the prior half-life parameter (a mean of around 15 days), the posterior values (7.9 days) decreased substantially, indicating an increase in the renal elimination of PFOA. The major reason for this is due to the significant increase in the renal clearance rate constant  $(P_{\rm b}^{\rm clear})$  and the decrease in both the renal reabsorption rate  $(P_b^{\text{reab}})$  and efflux rate  $(P_b^{\text{efflux}})$ , as shown in Table 3. All those active transport processes were facilitated by different transporters. Although a total of five transporters were considered for the renal elimination process, other transporters such as Oatp4c1<sup>57</sup> and multidrug resistance-associated proteins (Mrps)<sup>58</sup> located at the proximal tubular cells were not included due to limited information on their transport kinetics. However, our model results indicate that those transporters have the potential to significantly affect the elimination of PFOA and more in vitro data are needed.

4.2. Tissue Distribution of PFOA. Our model can successfully predict the tissue distribution patterns for PFOA in long-term simulations (i.e., after 12 or 28 days): liver > kidney  $\approx$  blood > gut > muscle  $\approx$  adipose. This pattern can be explained with the protein binding in those tissues. As described in eq 3, the protein binding for PFOA is determined by both the equilibrium association constant and the protein concentration in tissues. A strong association constant and high protein concentration results in high bioaccumulation of PFOA. Liver tissue has abundant LFABP and the association constant of LFABP is quite strong (the median of the posterior distribution is  $1.4 \times 10^5$  M<sup>-1</sup>, Table 3), which results in the highest accumulation of PFOA in liver. The kidney tissue also contains LFABP, but its concentration is much lower than that of liver; moreover, the kidney has high concentration of  $\alpha 2\mu$ globulin (with a weak association constant of  $5 \times 10^2 \text{ M}^{-1}$ ).  $^{40}$ For a blood tissue, it has abundant serum albumin, but the association constant of albumin (the median of the posterior distribution is  $3.6 \times 10^4 \,\mathrm{M}^{-1}$ , Table 3) is a little weaker than LFABP. These protein binding data show that kidney and blood are important accumulation sites for PFOA, but they contain less PFOA compared to liver tissue. For other tissues

(i.e., gut, muscle and adipose), there is only a small amount of albumin in their vascular space and interstitial fluid compartments; therefore, they have much lower concentrations of PFOA.

For the short-term dosing case (i.e., the 2 h experiment from Kudo et al.<sup>32</sup>), the PBPK model did not perform as well as for the long-term dosing simulation. The PFOA concentration in the liver was substantially underestimated by the model, while for gut and adipose, the PFOA concentration was overestimated by the model. This disagreement for the short-term dosing case could be caused by the parameterization of the surface area of those tissues or of passive diffusion. In addition, the underestimation of PFOA in liver could be attributed to cellular membrane association of PFOA at the beginning phase of distribution to the liver. In fact, Kudo et al. 32 showed that 2 h after dosing, around 97% of PFOA was found in the membrane fraction. Therefore, PFOA might sorb to some membrane components (e.g., protein or phospholipids<sup>59</sup>), which slows down the distribution of PFOA to liver over a short period. In the long-term simulation, it seems the membrane binding of PFOA has a negligible effect on the tissue distribution (Figure 4).

4.3. Model Limitations. The first limitation of the Bayesian framework is that prior knowledge is very limited for some model parameters, especially those related to protein binding and active transport processes. For example, the active efflux transporters Mrps, which are located at both the basolateral and apical membranes of proximal tubular cells, are dominant in female rats and could also be responsible for the substantial gender difference in PFOA elimination between male and female rats.<sup>39,58</sup> However, due to the lack of information on the transport kinetics of Mrps, a female rat model for PFOA was not considered in this study. In addition, the computational cost of MCMC simulations is very large, especially for a complex PBPK model. In this study, all the physiological parameters were fixed during the MCMC simulation to reduce the computational burden, so the opportunity to refine all parameters in the model was missed.

**4.4. Call for Data.** More data are required to further improve the PBPK model and generalize it to other species and other PFAS. First, data are needed on more PFAS-protein interactions, such as the Mrps transporters, which have the potential to significantly affect PFAS elimination, but for which very limited information is currently available. Given the importance of the equilibrium association constant of albumin with PFOA in the PBPK model, further more accurate measurements are also necessary for model validation. PFASprotein interaction data could be obtained through in vitro studies or estimated with molecular modeling tools (e.g., molecular docking and molecular dynamics). Finally, more in vivo toxicokinetic data on PFAS are needed for the Bayesian analysis of the PBPK model. As shown in Figure 3, even under the same dose scenarios, there is a substantial difference between the toxicokinetics data from Kim et al.33 and Kemper.<sup>31</sup> We need more experimental data to reduce the variability in observations, as well as to better understand actual inter-individual and intrapopulation variability.

#### ASSOCIATED CONTENT

## **5** Supporting Information

The Supporting Information is available free of charge at https://pubs.acs.org/doi/10.1021/acs.chemrestox.1c00193.

Additional information on rat model structure, physiological parameters for the male rat, mechanism-related parameters (*i.e.*, protein binding, passive diffusion, and active transport) for PFOA, mass balance equations for the PBPK model, convergence results for MCMC simulations, percentiles of the posterior distribution for the population mean and variance of each model parameter, trace plots of the MCMC simulation for selected model parameters, PFOA terminal tissue distributions under different dose scenarios, descriptions of the experimental data, and an "MCMC" folder containing experimental data files and the PBPK model code (mcmc.R) (PDF)

#### (ZIP)

## AUTHOR INFORMATION

#### **Corresponding Author**

Carla A. Ng — Department of Civil and Environmental Engineering, University of Pittsburgh, Pittsburgh, Pennsylvania 15261, United States; Secondary Appointment, Department of Environmental and Occupational Health, Graduate School of Public Health, University of Pittsburgh, Pittsburgh, Pennsylvania 15261, United States; ◎ orcid.org/0000-0001-5521-7862; Phone: 412-383-4075; Email: carla.ng@pitt.edu; Fax: 412-624-0135

### **Author**

Weixiao Cheng – Department of Civil and Environmental Engineering, University of Pittsburgh, Pittsburgh, Pennsylvania 15261, United States

Complete contact information is available at: https://pubs.acs.org/10.1021/acs.chemrestox.1c00193

## **Funding**

The authors acknowledge support from National Science Foundation, funding number: 1845336.

#### Notes

The authors declare no competing financial interest.

# REFERENCES

- (1) Wang, Z.; Cousins, I. T.; Scheringer, M.; Buck, R. C.; Hungerbühler, K. Global emission inventories for C4–C14 perfluoroalkyl carboxylic acid (PFCA) homologues from 1951 to 2030, Part I: production and emissions from quantifiable sources. *Environ. Int.* **2014**, *70*, 62–75.
- (2) Wang, Z.; DeWitt, J. C.; Higgins, C. P.; Cousins, I. T. A neverending story of per- and polyfluoroalkyl substances (PFASs)? *Environ. Sci. Technol.* **2017**, *51*, 2508–2518.
- (3) Lau, C.; Anitole, K.; Hodes, C.; Lai, D.; Pfahles-Hutchens, A.; Seed, J. Perfluoroalkyl acids: a review of monitoring and toxicological findings. *Toxicol. Sci.* **2007**, *99*, 366–394.
- (4) Krafft, M. P.; Riess, J. G. Per- and polyfluorinated substances (PFASs): Environmental challenges. *Curr. Opin. Colloid Interface Sci.* **2015**, 20, 192–212.
- (5) Kannan, K. Perfluoroalkyl and polyfluoroalkyl substances: current and future perspectives. *Environ. Chem.* **2011**, *8*, 333–338.
- (6) Olsen, G. W.; Burris, J. M.; Ehresman, D. J.; Froehlich, J. W.; Seacat, A. M.; Butenhoff, J. L.; Zobel, L. R. Half-life of serum elimination of perfluorooctanesulfonate, perfluorohexanesulfonate, and perfluorooctanoate in retired fluorochemical production workers. *Environ. Health Perspect.* **2007**, *115*, 1298–1305.
- (7) Macon, M. B.; Villanueva, L. R.; Tatum-Gibbs, K.; Zehr, R. D.; Strynar, M. J.; Stanko, J. P.; White, S. S.; Helfant, L.; Fenton, S. E. Prenatal perfluorooctanoic acid exposure in CD-1 mice: low-dose

- developmental effects and internal dosimetry. *Toxicol. Sci.* **2011**, *122*, 134–145.
- (8) National Toxicology Program (NTP). NTP Technical Report on the Toxicity Studies of Perfluoroalkyl Carboxylates (Perfluorohexanoic Acid, Perfluorooctanoic Acid, Perfluorononanoic Acid, and Perfluorodecanoic Acid) Administered by Gavage to Sprague Dawley (Hsd:Sprague Dawley SD) Rats; Toxicity Report 97, 2019.
- (9) Fenton, S. E.; Ducatman, A.; Boobis, A.; DeWitt, J. C.; Lau, C.; Ng, C.; Smith, J. S.; Roberts, S. M. Per- and polyfluoroalkyl substance toxicity and human health review: Current state of knowledge and strategies for informing future research. *Environ. Toxicol. Chem.* **2021**, 40, 606–630.
- (10) Wang, Z.; Cousins, I. T.; Scheringer, M.; Hungerbuehler, K. Hazard assessment of fluorinated alternatives to long-chain perfluoroalkyl acids (PFAAs) and their precursors: status quo, ongoing challenges and possible solutions. *Environ. Int.* **2015**, *75*, 172–179.
- (11) Loccisano, A. E.; Campbell, J. L.; Butenhoff, J. L.; Andersen, M. E.; Clewell, H. J. Comparison and evaluation of pharmacokinetics of PFOA and PFOS in the adult rat using a physiologically based pharmacokinetic model. *Reprod. Toxicol.* **2012**, *33*, 452–467.
- (12) Tan, Y.-M.; Clewell, H. J.; Andersen, M. E. Time dependencies in perfluorooctylacids disposition in rat and monkeys: a kinetic analysis. *Toxicol. Lett.* **2008**, *177*, 38–47.
- (13) Worley, R. R.; Fisher, J. Application of physiologically-based pharmacokinetic modeling to explore the role of kidney transporters in renal reabsorption of perfluorooctanoic acid in the rat. *Toxicol. Appl. Pharmacol.* **2015**, 289, 428–441.
- (14) Fàbrega, F.; Kumar, V.; Schuhmacher, M.; Domingo, J. L.; Nadal, M. PBPK modeling for PFOS and PFOA: Validation with human experimental data. *Toxicol. Lett.* **2014**, 230, 244–251.
- (15) Fàbrega, F.; Kumar, V.; Benfenati, E.; Schuhmacher, M.; Domingo, J. L.; Nadal, M. Physiologically based pharmacokinetic modeling of perfluoroalkyl substances in the human body. *Toxicol. Environ. Chem.* **2015**, 97, 814–827.
- (16) Loccisano, A. E.; Campbell, J. L.; Andersen, M. E.; Clewell, H. J. Evaluation and prediction of pharmacokinetics of PFOA and PFOS in the monkey and human using a PBPK model. *Regul. Toxicol. Pharmacol.* **2011**, *59*, 157–175.
- (17) Andersen, M. E.; Clewell, H. J.; Tan, Y.-M.; Butenhoff, J. L.; Olsen, G. W. Pharmacokinetic modeling of saturable, renal resorption of perfluoroalkylacids in monkeys—probing the determinants of long plasma half-lives. *Toxicology* **2006**, 227, 156–164.
- (18) Armitage, J. M.; Erickson, R. J.; Luckenbach, T.; Ng, C. A.; Prosser, R. S.; Arnot, J. A.; Schirmer, K.; Nichols, J. W. Assessing the bioaccumulation potential of ionizable organic compounds: Current knowledge and research priorities. *Environ. Toxicol. Chem.* **2017**, *36*, 882–897
- (19) Lin, Z.; Gehring, R.; Mochel, J. P.; Lavé, T.; Riviere, J. E. Mathematical modeling and simulation in animal health—Part II: principles, methods, applications, and value of physiologically based pharmacokinetic modeling in veterinary medicine and food safety assessment. *J. Vet. Pharmacol. Ther.* **2016**, 39, 421–438.
- (20) Ng, C. A.; Hungerbühler, K. Bioconcentration of perfluorinated alkyl acids: how important is specific binding? *Environ. Sci. Technol.* **2013**, *47*, 7214–7223.
- (21) Cheng, W.; Ng, C. A. A Permeability-Limited Physiologically Based Pharmacokinetic (PBPK) Model for Perfluorooctanoic acid (PFOA) in Male Rats. *Environ. Sci. Technol.* **2017**, *51*, 9930–9939.
- (22) Han, X.; Snow, T. A.; Kemper, R. A.; Jepson, G. W. Binding of perfluorooctanoic acid to rat and human plasma proteins. *Chem. Res. Toxicol.* **2003**, *16*, 775–781.
- (23) Woodcroft, M. W.; Ellis, D. A.; Rafferty, S. P.; Burns, D. C.; March, R. E.; Stock, N. L.; Trumpour, K. S.; Yee, J.; Munro, K. Experimental characterization of the mechanism of perfluorocarboxylic acids' liver protein bioaccumulation: The key role of the neutral species. *Environ. Toxicol. Chem.* **2010**, *29*, 1669–1677.
- (24) Hebert, P. C.; MacManus-Spencer, L. A. Development of a fluorescence model for the binding of medium-to long-chain perfluoroalkyl acids to human serum albumin through a mechanistic

- evaluation of spectroscopic evidence. Anal. Chem. 2010, 82, 6463-6471.
- (25) Luebker, D. J.; Hansen, K. J.; Bass, N. M.; Butenhoff, J. L.; Seacat, A. M. Interactions of flurochemicals with rat liver fatty acid-binding protein. *Toxicology* **2002**, *176*, 175–185.
- (26) Han, X.; Yang, C.-H.; Snajdr, S. I.; Nabb, D. L.; Mingoia, R. T. Uptake of perfluorooctanoate in freshly isolated hepatocytes from male and female rats. *Toxicol. Lett.* **2008**, *181*, 81–86.
- (27) Weaver, Y. M.; Ehresman, D. J.; Butenhoff, J. L.; Hagenbuch, B. Roles of rat renal organic anion transporters in transporting perfluorinated carboxylates with different chain lengths. *Toxicol. Sci.* **2009**, *113*, 305–314.
- (28) Yang, C.-H.; Glover, K. P.; Han, X. Organic anion transporting polypeptide (Oatp) 1a1-mediated perfluorooctanoate transport and evidence for a renal reabsorption mechanism of Oatp1a1 in renal elimination of perfluorocarboxylates in rats. *Toxicol. Lett.* **2009**, *190*, 163–171.
- (29) Yang, C.-H.; Glover, K. P.; Han, X. Characterization of cellular uptake of perfluorooctanoate via organic anion-transporting polypeptide 1A2, organic anion transporter 4, and urate transporter 1 for their potential roles in mediating human renal reabsorption of perfluorocarboxylates. *Toxicol. Sci.* **2010**, *117*, 294–302.
- (30) Chou, W.-C.; Lin, Z. Bayesian evaluation of a physiologically based pharmacokinetic (PBPK) model for perfluorooctane sulfonate (PFOS) to characterize the interspecies uncertainty between mice, rats, monkeys, and humans: Development and performance verification. *Environ. Int.* **2019**, *129*, 408–422.
- (31) Kemper, R. A. Perfluorooctanoic Acid: Toxicokinetics in the Rat; DuPont Project ID: 7473, 2003.
- (32) Kudo, N.; Sakai, A.; Mitsumoto, A.; Hibino, Y.; Tsuda, T.; Kawashima, Y. Tissue distribution and hepatic subcellular distribution of perfluorooctanoic acid at low dose are different from those at high dose in rats. *Biol. Pharm. Bull.* **2007**, *30*, 1535–1540.
- (33) Kim, S.-J.; Heo, S.-H.; Lee, D.-S.; Hwang, I. G.; Lee, Y.-B.; Cho, H.-Y. Gender differences in pharmacokinetics and tissue distribution of 3 perfluoroalkyl and polyfluoroalkyl substances in rats. *Food Chem. Toxicol.* **2016**, *97*, 243–255.
- (34) Bernillon, P.; Bois, F. Y. Statistical issues in toxicokinetic modeling: a Bayesian perspective. *Environ. Health Perspect.* **2000**, *108*, 883–893.
- (35) Hack, C. E.; Chiu, W. A.; Zhao, Q. J.; Clewell, H. J. Bayesian population analysis of a harmonized physiologically based pharmacokinetic model of trichloroethylene and its metabolites. *Regul. Toxicol. Pharmacol.* **2006**, *46*, 63–83.
- (36) Vestergren, R.; Cousins, I. T. Tracking the pathways of human exposure to perfluorocarboxylates. *Environ. Sci. Technol.* **2009**, 43, 5565–5575.
- (37) Conder, J. M.; Hoke, R. A.; de Wolf, W.; Russell, M. H.; Buck, R. C. Are PFCAs bioaccumulative? A critical review and comparison with regulatory criteria and persistent lipophilic compounds. *Environ. Sci. Technol.* **2008**, *42*, 995–1003.
- (38) Zhao, W.; Zitzow, J. D.; Ehresman, D. J.; Chang, S.-C.; Butenhoff, J. L.; Forster, J.; Hagenbuch, B. Na+/taurocholate cotransporting polypeptide and apical sodium-dependent bile acid transporter are involved in the disposition of perfluoroalkyl sulfonates in humans and rats. *Toxicol. Sci.* 2015, 146, 363–373.
- (39) Han, X.; Nabb, D. L.; Russell, M. H.; Kennedy, G. L.; Rickard, R. W. Renal elimination of perfluorocarboxylates (PFCAs). *Chem. Res. Toxicol.* **2011**, 25, 35–46.
- (40) Han, X.; Hinderliter, P. M.; Snow, T. A.; Jepson, G. W. Binding of Perfluorooctanoic Acid to Rat Liver-form and Kidney-form  $\alpha$ 2u-Globulins. *Drug Chem. Toxicol.* **2004**, *27*, 341–360.
- (41) Gad, S. C. ADME and Biopharmaceutical Properties; Wiley, 2008.
- (42) Ebert, A.; Allendorf, F.; Berger, U.; Goss, K.-U.; Ulrich, N. Membrane/water partitioning and permeabilities of perfluoroalkyl acids and four of their alternatives and the effects on toxicokinetic behavior. *Environ. Sci. Technol.* **2020**, *54*, 5051–5061.

- (43) MacLeod, M.; Fraser, A. J.; Mackay, D. Evaluating and expressing the propagation of uncertainty in chemical fate and bioaccumulation models. *Environ. Toxicol. Chem.* **2002**, 21, 700–709.
- (44) Haario, H.; Laine, M.; Mira, A.; Saksman, E. DRAM: efficient adaptive MCMC. Stat. Comput. 2006, 16, 339-354.
- (45) Roy, V. Convergence diagnostics for Markov chain Monte Carlo. Annu. Rev. Stat. Appl. 2020, 7, 387–412.
- (46) Gelman, A.; Carlin, J. B.; Stern, H. S.; Dunson, D. B.; Vehtari, A.; Rubin, D. B. *Bayesian Data Analysis*; CRC Press, 2013.
- (47) Spruill, W.; Wade, W.; DiPiro, J. T.; Blouin, R. A.; Pruemer, J. M. Concepts in Clinical Pharmacokinetics; ASHP, 2014.
- (48) Soetaert, K.; Petzoldt, T. Inverse modelling, sensitivity and Monte Carlo analysis in R using package FME. *J. Stat. Software* **2010**, 33, 1–28.
- (49) Yang, Y.; Xu, X.; Georgopoulos, P. G. A Bayesian population PBPK model for multiroute chloroform exposure. *J. Exposure Sci. Environ. Epidemiol.* **2010**, 20, 326–341.
- (50) Ohmori, K.; Kudo, N.; Katayama, K.; Kawashima, Y. Comparison of the toxicokinetics between perfluorocarboxylic acids with different carbon chain length. *Toxicology* **2003**, *184*, 135–140.
- (51) Heuvel, J. P. V.; Kuslikis, B. I.; Van Rafelghem, M. J.; Peterson, R. E. Tissue distribution, metabolism, and elimination of perfluor-ooctanoic acid in male and female rats. *J. Biochem. Toxicol.* **1991**, *6*, 83–92.
- (52) Harada, K.; Inoue, K.; Morikawa, A.; Yoshinaga, T.; Saito, N.; Koizumi, A. Renal clearance of perfluorooctane sulfonate and perfluorooctanoate in humans and their species-specific excretion. *Environ. Res.* **2005**, *99*, 253–261.
- (53) Benskin, J. P.; De Silva, A. O.; Martin, L. J.; Arsenault, G.; McCrindle, R.; Riddell, N.; Mabury, S. A.; Martin, J. W. Disposition of perfluorinated acid isomers in sprague-dawley rats; Part 1: Single dose. *Environ. Toxicol. Chem.* **2009**, 28, 542–554.
- (54) Wambaugh, J. F.; Barton, H. A.; Setzer, R. W. Comparing models for perfluorooctanoic acid pharmacokinetics using Bayesian analysis. *J. Pharmacokinet. Pharmacodyn.* **2008**, *35*, 683–712.
- (55) Wu, L.-L.; Gao, H.-W.; Gao, N.-Y.; Chen, F.-F.; Chen, L. Interaction of perfluorooctanoic acid with human serum albumin. *BMC Struct. Biol.* **2009**, *9*, 31.
- (56) Qin, P.; Liu, R.; Pan, X.; Fang, X.; Mou, Y. Impact of carbon chain length on binding of perfluoroalkyl acids to bovine serum albumin determined by spectroscopic methods. *J. Agric. Food Chem.* **2010**, 58, 5561–5567.
- (57) Mikkaichi, T.; Suzuki, T.; Onogawa, T.; Tanemoto, M.; Mizutamari, H.; Okada, M.; Chaki, T.; Masuda, S.; Tokui, T.; Eto, N.; Abe, M.; Satoh, F.; Unno, M.; Hishinuma, T.; Inui, K.-i.; Ito, S.; Goto, J.; Abe, T. Isolation and characterization of a digoxin transporter and its rat homologue expressed in the kidney. *Proc. Natl. Acad. Sci. U.S.A.* **2004**, *101*, 3569–3574.
- (58) Sabolić, I.; Asif, A. R.; Budach, W. E.; Wanke, C.; Bahn, A.; Burckhardt, G. Gender differences in kidney function. *Pflugers Arch* **2007**, 455, 397–429.
- (59) Armitage, J. M.; Arnot, J. A.; Wania, F.; Mackay, D. Development and evaluation of a mechanistic bioconcentration model for ionogenic organic chemicals in fish. *Environ. Toxicol. Chem.* **2013**, 32, 115–128.